Proceedings of the ASME-JSME-KSME Joint Fluids Engineering Conference 2015
AJK2015-FED
July 26-31, 2015, SEOUL, KOREA

AJK2015-02061

INVESTIGATION OF UNSTEADY TIP CLEARANCE FLOW IN A LOW-SPEED ONE AND HALF STAGE AXIAL COMPRESSOR WITH LES AND PIV

Chunill Hah, Michael Hathaway
NASA Glenn Research Center,
Cleveland, Ohio

Joseph Katz, David Tan
Johns Hopkins University
Baltimore, Maryland

ABSTRACT

The primary focus of this paper is to investigate how a rotor's unsteady tip clearance flow structure changes in a low speed one and half stage axial compressor when the rotor tip gap size is increased from 0.5 mm (0.49% of rotor tip blade chord, 2% of blade span) to 2.4 mm (2.34% chord, 4% span) at the design condition are investigated. The changes in unsteady tip clearance flow with the 0.62 % tip gap as the flow rate is reduced to near stall condition are also investigated. A Large Eddy Simulation (LES) is applied to calculate the unsteady flow field at these three flow conditions. Detailed Stereoscopic PIV (SPIV) measurements of the current flow fields were also performed at the Johns Hopkins University in a refractive index-matched test facility which renders the compressor blades and casing optically transparent. With this setup, the unsteady velocity field in the entire flow domain, including the flow inside the tip gap, can be measured. Unsteady tip clearance flow fields from LES are compared with the PIV measurements and both LES and PIV results are used to study changes in tip clearance flow structures.

The current study shows that the tip clearance vortex is not a single structure as traditionally perceived. The tip clearance vortex is formed by multiple interlaced vorticities. Therefore, the tip clearance vortex is inherently unsteady.

The multiple interlaced vortices never roll up to form a single structure. When phased-averaged, the tip clearance vortex appears as a single structure. When flow rate is reduced with the same tip gap, the tip clearance vortex rolls further upstream and the tip clearance vortex moves further radially inward and away from the suction side of the blade. When the tip gap size is increased at the design flow condition, the overall tip clearance vortex becomes stronger and it stays closer to the blade suction side and the vortex core extends all the way to the exit of the blade passage.

Measured and calculated unsteady flow fields inside the tip gap agree fairly well. Instantaneous velocity vectors inside the tip gap from both the PIV and LES do show flow separation and reattachment at the entrance of tip gap as some earlier studies suggested. This area at the entrance of tip gap flow (the pressure side of the blade) is confined very close to the rotor tip section. With a small tip gap (0.5mm), the gap flow looks like a simple two-dimensional channel flow with larger velocity near the casing for both flow rates. A small area with a sharp velocity gradient is observed just above the rotor tip. This strong shear layer is turned radially inward when it collides with the incoming flow and forms the core structure of the tip clearance vortex. When tip gap size is increased to 2.4 mm at the design operation, the radial profile of the tip gap flow changes drastically. With the large tip gap, the gap flow looks like a two-dimensional channel flow only near the casing. Near the rotor top section, a bigger region with very large shear and reversed flow is observed.

INTRODUCTION

Tip clearance flow plays an important role in the operation of axial compressors. When the tip clearance becomes larger during the service life of an engine, both the efficiency at the design condition and the stall margin deteriorate. Many experimental and analytical studies to understand tip clearance flows have been reported (for example, Hah [1987], Hoeing et al. [1993], Vo et al. [1998], Inoue et al. [2004], Chen et al. [2008], Weichert and Day [2012], Yamada et al. [2013], etc.). However, details of the unsteady tip clearance flow structure and its change with the tip gap size or operating condition are not well known.

Tip clearance flow arises due to the pressure difference between the pressure and suction sides of the blade in the tip gap area. Flow through the tip gap interacts with the incoming passage flow near the suction side of the blade as it leaves the blade tip section, forming the tip clearance vortex. The vortex core is formed by fluid originating from near the leading edge of the blade. Fluid flowing over the remainder of the blade rolls around this core vortex and adds swirl intensity. Some tip clearance flow originating near the casing travels over to the tip gap of the adjacent blade, resulting in a so-called double leakage flow (Smith [1993]). Tip clearance flow has been handled as a steady flow phenomenon for many applications. However, tip clearance flow in a compressor is not steady, even at design

operation, due to vortex shedding at the trailing edge and the oscillation of the tip leakage vortex, as well as flow field interactions from adjacent blade rows. Bergner et al. [2006] measured the instantaneous pressure difference between the blade suction side and pressure side near the leading edge at near stall operation. They reported that the pressure difference changes constantly and the pressure difference even occasionally becomes negative during near stall operation, which indicates that the formation of the tip clearance flow is also transient and the tip leakage vortex itself is formed intermittently.

The effect of the rotor tip gap size on the compressor flow field has been widely investigated. Several previous studies (Mailach et al. [2000], Maertz et al. [2002], Kiel et al. [2003], Inoue et al. [2004], etc.) reported that rotating instability occurs when the tip gap is increased in axial compressors. As the resulting non-synchronous blade vibration affects engine safety, many studies have been reported. Maertz et al. [2002] reported that the movement of the instability vortex along the leading edge plane is the main cause of instability during the compressor operation at near stall operation. Inoue et al. [2004] and Yamada et al. [2013] reported formation of a tornado-type vortex near the suction surface and subsequent vortex breakup as the main mechanism of the flow at near stall operation with a large tip gap.

Although significant progress has been made in the experimental investigation of tip gap flow lately, direct measurement of the unsteady flow field inside the rotor tip gap has not been possible. A new program to investigate the unsteady tip clearance flow in a low speed one and a half stage axial compressor was initiated under the auspices of the NASA Fixed Wing Project to understand and mitigate losses associated with large rotor tip gaps of N+3 relevant small, high overall pressure ratio compressor aft stages. Detailed measurements of the unsteady tip clearance flows at two tip clearances (0.5 mm and 2.4 mm, 0.49% and 2.34% rotor tip chord) have been performed with three-dimensional PIV in a refractive index-matched test facility at the Johns Hopkins University. Details of the PIV procedure are given by Wu et al. [2011]. The primary focus of the program is to study the detailed unsteady flow structures in the tip gap at the design and near stall operation with two tip gap sizes. The same flows in the one and half stage axial compressor were analyzed with a Large Eddy Simulation (LES).

The primary focus of the current study is to investigate changes in the detailed tip clearance flow structure in the one and a half stage axial compressor when the tip gap size is increased about five times at the design flow rate and when the flow rate is decreased to near stall operation with the original tip gap.

ONE AND A HALF STAGE LOW-SPEED AXIAL COMPRESSOR FOR TIP GAP FLOW RESEARCH

The design intent for the John's Hopkins University (JHU) compressor, which is focused on investigating the flow physics of the rotor tip clearance flow field, was for it to be an aerodynamically scaled derivative of the first one and a half stages (i.e., inlet guide vane, rotor, and stator) of the NASA Glenn Research Center's Low-Speed Axial Compressor (LSAC), which comprises an IGV followed by four geometrically identical stages designed for accurate low-speed simulation of a high-speed multistage core compressor (Wasserbauer, 1995). In addition, commensurate with the NASA LSAC compressor, the JHU compressor should have a long entrance length to develop thick endwall boundary layers typical of an embedded stage. The NASA LSAC blades themselves were aerodynamically scaled and modeled after General Electric's Energy Efficient Engine blading (Wisler, 1977), with modifications to the original GE blade geometry to account for differences in the hub-to-tip ratios of the two compressors (Wellborn, 1996). The JHU, LSAC, and GE compressor design heritage therefore provides potential for continuity of physics insight obtained from these related, but different compressors. The JHU compressor was sized to a 9" (22.86 cm) casing flow path radius to be compatible with the JHU compressor facility hardware, and was initially

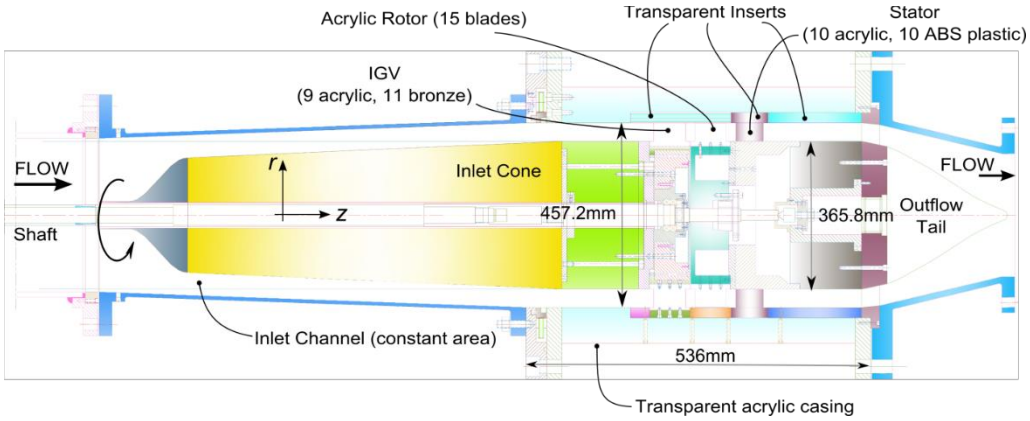

FIGURE 1. CROSS SECTION OF TEST COMPRESSOR FACILITY

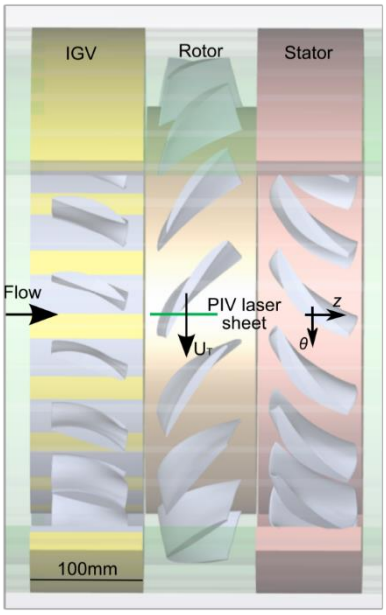

FIGURE 2. VIEW OF ONE AND A HALF STAGE COMPRESSOR

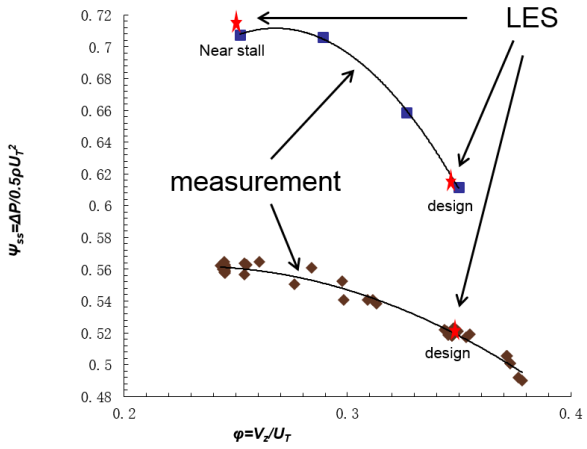

FIGURE 3. PRESSURE RISE CHARACTERISTICS

mechanically scaled from the NASA LSAC 24" (60.96 cm) casing radius. However, a direct mechanical scale yields a rotor blade tip thickness that was too thin to withstand the stresses associated with operation in the much higher density NaI-H2O mixture of the working fluid at the desired 480 rpm design speed set by the facility power limitations. It was therefore necesary to increase the rotor blade tip thickness to 0.169" (4.3 mm) to withstand the higher stress at the rotor blade tip. Then, to maintain the LSAC rotor blade profile shape, and thus aerodynamic similarity with the LSAC, the JHU rotor was fixed to have the same rotor blade tip thickness to chord ratio as the

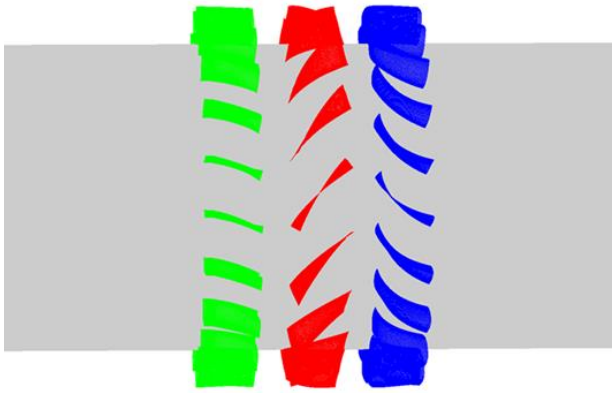

FIGURE 4. COMPUTATIONAL DOMAIN

NASA LSAC, and the rotor tip chord increased to achieve a 0.169" (4.3 mm) rotor blade tip thickness. The resultant rotor chord scaling was then used for the IGV, rotor, and stator, which yielded a longer axial chord, relative to a direct mechanical scale, and thus a much lower aspect ratio. Next, to maintain rotor tip solidity (recall the focus of the JHL rig is rotor tip clearance flow physics) the number of IGV, rotor, and stator blades were decreased, and then fixing the rotor count the IGV and Stator counts were slightly adjusted to achieve a 20 IGV, 15 rotor, and 20 stator blade count, which with a 3/4 ratio of rotor to IGV/Stator blade passages facilitates unsteady simulations. The target Reynolds number is 4.0×10^5 based on tip speed and the rotor chord length at the tip. Details of the design parameters are given by Tan et al. [2014].

Figure 1 shows the cross section of the test compressor. A view of the compressor test section is given in Figure 2. Two rotor blade tip gaps of 0.5 mm (0.49 % of tip chord) and 2.4 mm (2.34% of tip chord) were selected for the study. The compressor static pressure rise characteristic curves for two tip gaps are given in Figure 3. The current study aims to investigate changes in tip clearance flow when the tip gap is increased. For the present paper, detailed tip flows are examined at peak efficiency condition with two tip gaps (0.5 mm and 2.4 mm). Also, changes in tip flow when the flow rate is decreased to near stall condition with the 0.5 mm tip gap is studied. Static pressure rises from the LES simulation at the three operating conditions are marked in Figure 3.

NUMERICAL PROCEDURE

A Large Eddy Simulation (LES) was applied in the present study to calculate the unsteady flow and various vortex structures in the rotor tip gap. With spatially-filtered Navier-Stokes equations, the subgrid-scale stress tensor term must be modeled properly for closure of the governing equations. A Smagorinsky-type eddy-viscosity model was used for the subgrid stress tensor, and the standard dynamic model by Germano et al. [1991] was applied.

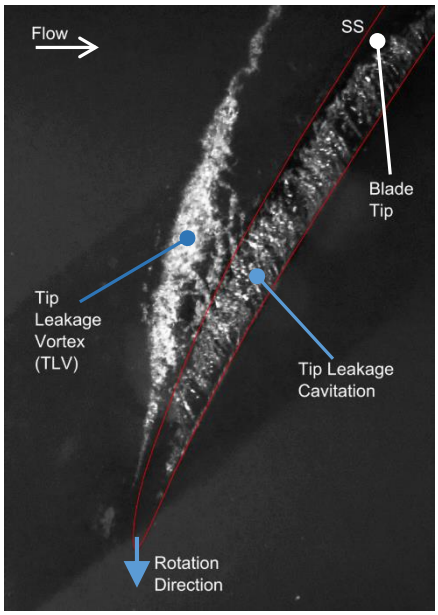

Cavitation visualization

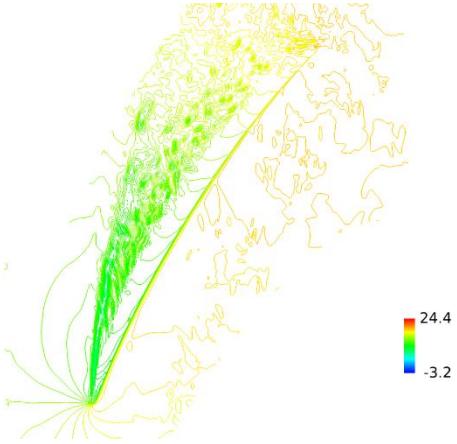

Static pressure from LES

FIGURE 5. COMPARISON OF TIP GAP FLOW STRUCTURE, 0.5 mm GAP, DESIGN CONDITION

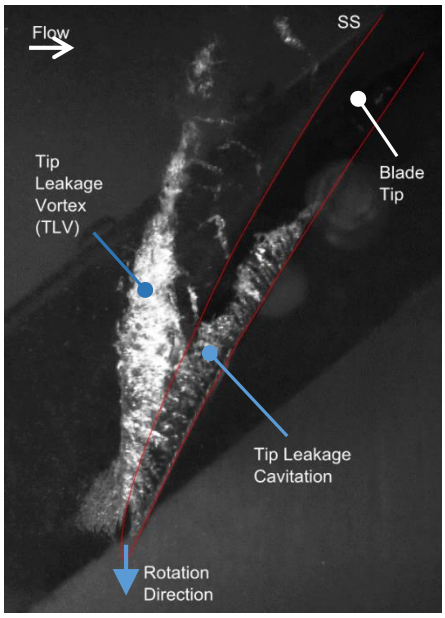

Cavitation visualization

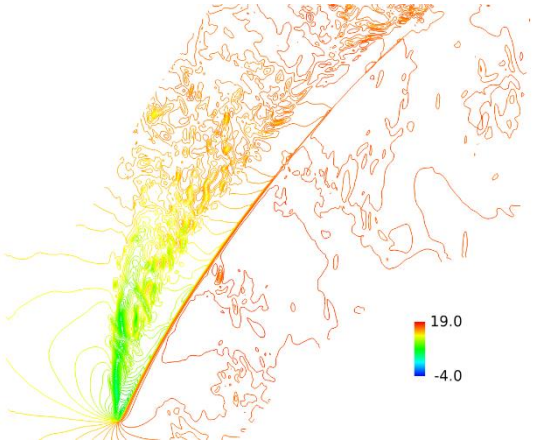

Static pressure from LES

FIGURE 6. COMPARISON OF TIP GAP FLOW STRUCTURE, 0.5 mm GAP, NEAR STALL CONDITION

In the current study, the governing equations are solved with a pressure-based implicit method using a fully conservative control volume approach. A third-order accurate interpolation scheme is used for the discretization of convection terms and central differencing is used for the diffusion terms. The method is of second-order accuracy with smoothly varying grids. For the time-dependent terms, an implicit second-order scheme is used and a number of sub-iterations are performed at each time step. About 6000 time steps are used for one rotor revolution.

Standard boundary conditions for the multi-blade rows were applied at the boundaries of the computational domain (Hah and Shin [2010]). The inflow boundary of the computational domain was located 20 average blade heights upstream of the rotor leading edge in order to damp out any possible reflections. Likewise, the outflow boundary was located 20 blade heights downstream from the trailing edge. Circumferentially averaged static pressure at the exit boundary casing was specified to control the mass flow rate. Non-reflecting boundary conditions were applied at the inlet and the exit boundaries.

The computational grid consists of 430 nodes in the blade-to-blade direction, 295 nodes in the spanwise direction, and 360 nodes in the streamwise direction for each blade passage. The

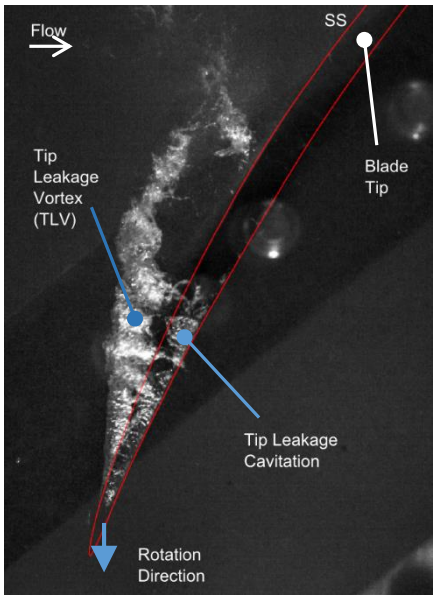

Cavitation visualization

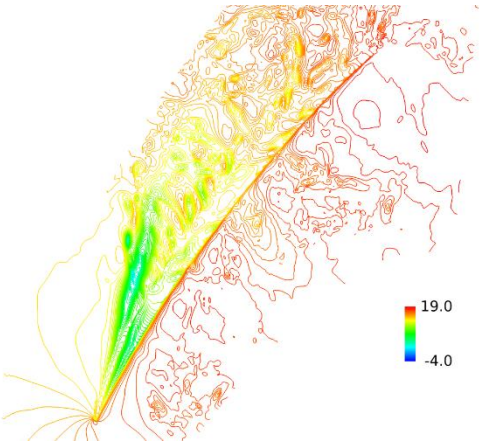

Static pressure from LES

FIGURE 7. COMPARISON OF TIP GAP FLOW STRUCTURE, 2.4 mm GAP, DESIGN CONDITION

rotor tip clearance geometry is represented by 56 nodes in the blade-to-blade direction, 75 nodes in the spanwise direction, and 30 nodes in the streamwise direction in an attempt to accurately resolve the tip clearance flow field. I-grid topology is used to reduce grid skewness, and a single-block grid is used. For the LES simulations, the number of blades was reduced from 20-15-20 to 4-3-4 with tangential periodicity condition. The grid size for the entire one and half stage is about 500 million nodes. The wall resolution is within the range Dx+ < 20, Dy+ <1.0, and Dz+ < 1.5 in the streamwise, pitchwise, and spanwise directions. The applied grid is not fine enough to resolve small length scales in the wall boundary layer. However, the current study is aimed to

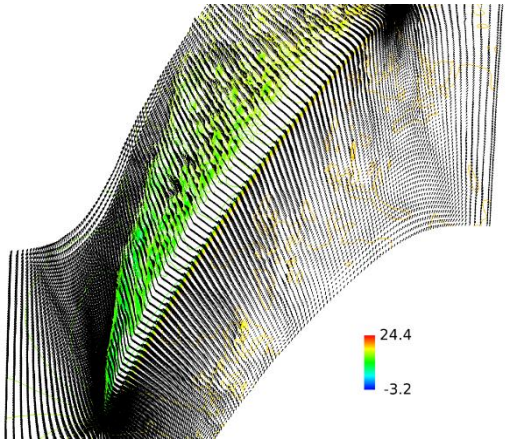

(a) 0.5 mm tip gap at design condition

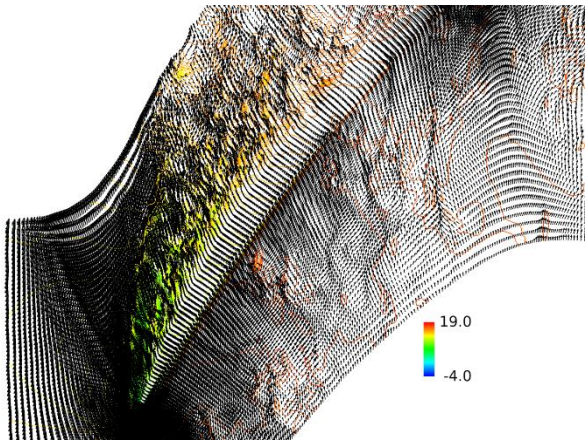

(b) 0.5 mm tip gap at near stall condition

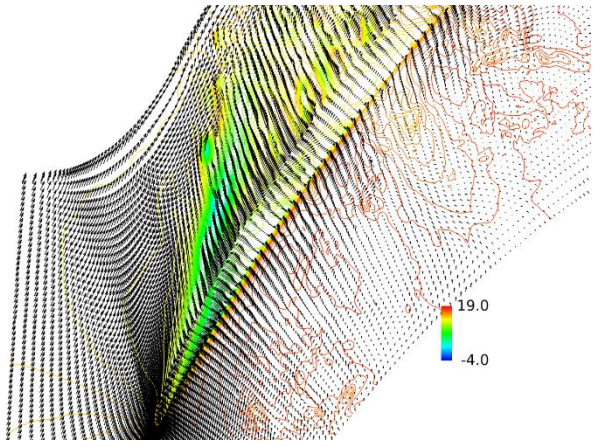

(c) 2.4 mm tip gap at design condition

FIGURE 8. INSTANTANEOUS VELOCITY VECTORS 0.02 mm ABOVE ROTOR TIP

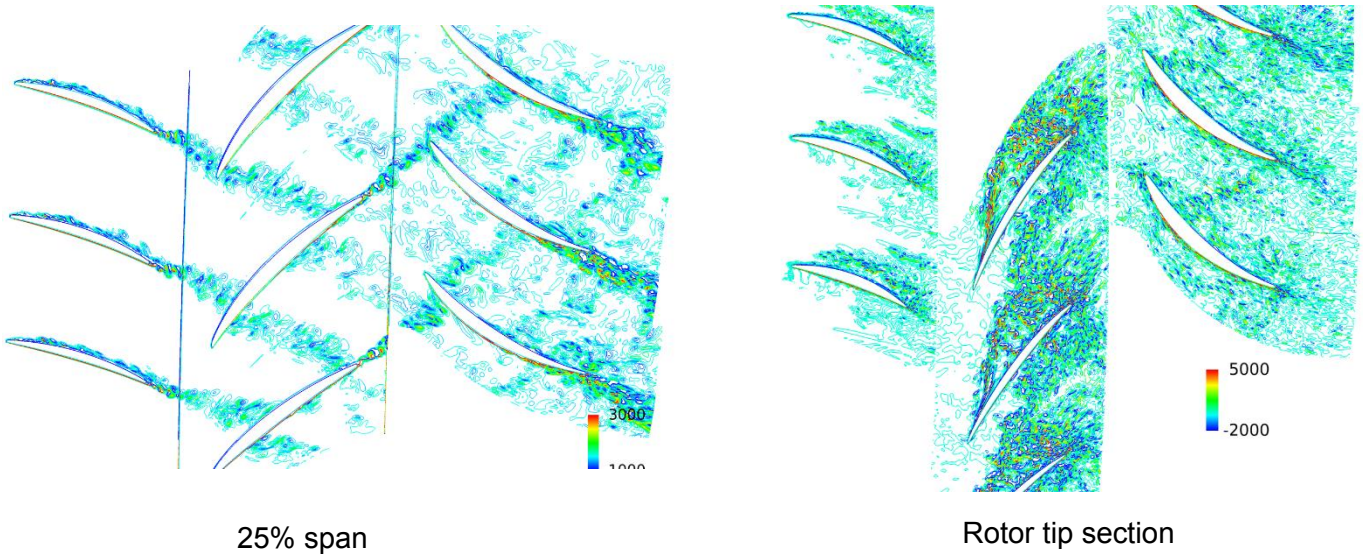

FIGURE 9. INSTANTANEOUS VORTICITY CONTOURS AT DESIGN CONDITION, 2.4 mm GAP

investigate tip clearance flow, which is formed away from the wall. Figure 4 shows the computational domain of the compressor stage.

All the computations were performed with NASA's Columbia supercomputer system, which allows parallel computation with up to 512 processors.

OVERALL TIP CLEARANCE FLOW STRUCTURE

Figures 5, 6 and 7 show the cavitation flow visualization of the tip clearance flow at three flow conditions. Instantaneous static pressure distributions at the rotor tip from LES are also compared with the flow visualization. Cavitation inception occurs when the local pressure drops below the vapor pressure. Therefore, the flow visualization in Figures 5-7 indicates areas with low pressure. Static pressure at the core of the tip clearance vortex is low. Consequently, the cavitation visualization in Figures 5-7 shows traces of the tip clearance vortex. Instantaneous static pressure fields from LES in Figures 5-7 agree fairly well with the cavitation flow visualization. As expected, the tip clearance core vortex, which forms along the plane where the tip clearance flow interacts with the main flow, becomes more tangential as the flow rate is decreased as shown in Figure 6. When the tip gap is increased from 0.5 mm to 2.4 mm, the tip clearance vortex becomes stronger. However, it stays closer to the blade suction surface.

Instantaneous velocity vectors near the rotor tip section (one computational node away from the tip section) are shown in Figure 8. When the flow rate is decreased from the peak efficiency to near stall with the 0.5 mm tip gap, tip clearance flow between the blade suction surface and the tip clearance core vortex becomes more turbulent according to the LES. This indicates more loss generation in the tip clearance flow region as the flow rate is decreased. When the tip gap is increased at the peak efficiency condition, a significant change is observed for the velocity vectors above the rotor tip. The velocity vectors in the tip gap are almost in the same direction with the 0.5 mm tip gap. However, instantaneous velocity vectors show large variation both in magnitude and direction with the 2.4 mm tip gap. At this radial location, some tip gap flow moves from the suction side to the pressure side. When the tip gap is increased, the pressure difference between the pressure side and the suction side oscillates with a large magnitude, as previously observed in other compressors (Bergner et al. [2006]), reversed tip gap flow could be observed.

Contours of vorticity at 25% span and at the rotor tip section at the peak efficiency condition with 2.4 mm tip gap from LES are given in Figure 9. At 25 % span, wakes from the IGV interact with the rotor blade, and traditional IGV/rotor interaction is clearly observed. On the other hand, the IGV wake decays rapidly at the rotor tip section and the influence of IGV wake on the rotor seems very small near the casing. The vorticity contours at the rotor tip section in Figure 9 illustrate many vortex structures and interactions among these vorticities. Also, this indicates most of the loss is generated in the area between the blade suction side and the tip clearance core vortex well behind the leading edge at this flow condition. The tip clearance core vortex itself generates a small fraction of total loss due to the tip clearance flow.

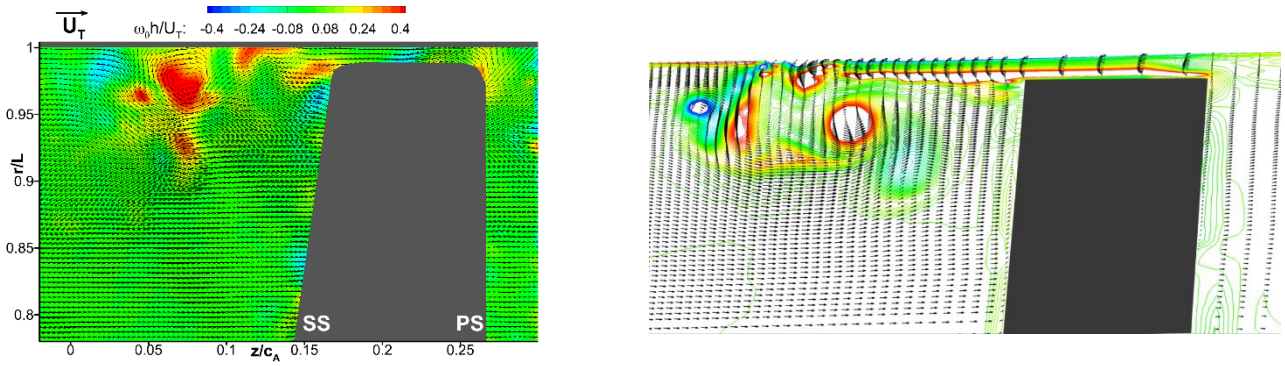

FIGURE 10. COMPARISON OF INSTANTANEOUS VELOCITY VECTORS AND VORTICITY, s/C = 0.328, 0.5 mm GAP, AT DESIGN CONDITION

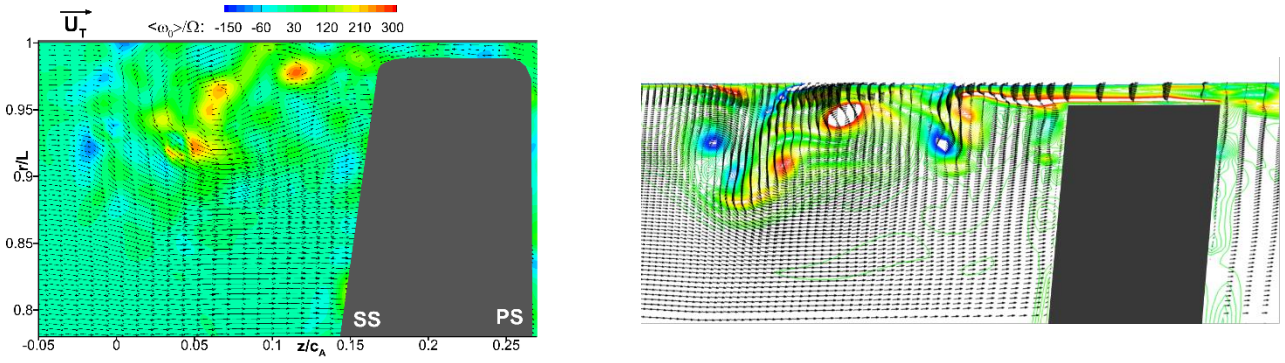

FIGURE 11. COMPARISON OF INSTANTANEOUS VELOCITY VECTORS AND VORTICITY, s/C = 0.328, 0.5 mm GAP, AT NEAR STALL CONDITION

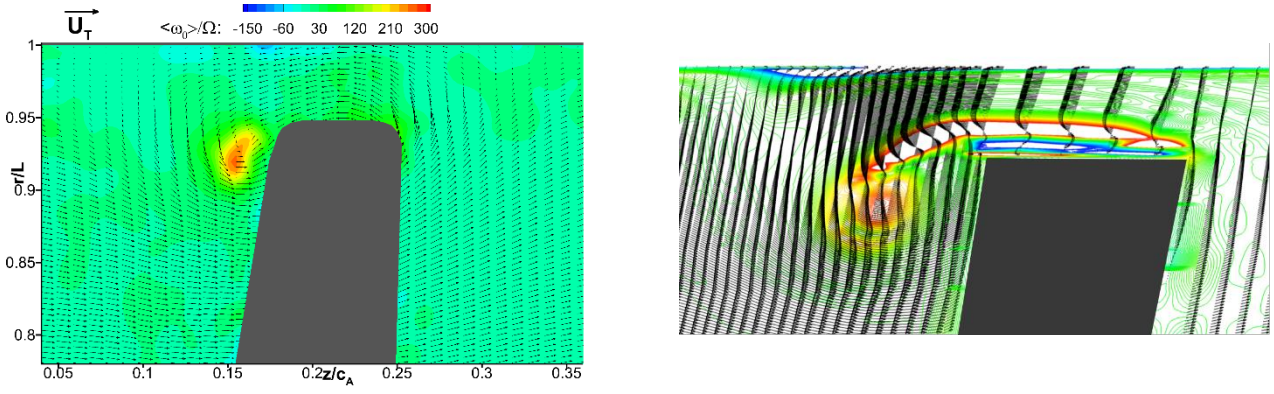

FIGURE 12. COMPARISON OF INSTANTANEOUS VELOCITY VECTORS AND VORTICITY, s/C = 0.328, 2.4 mm GAP, AT DESIGN CONDITION

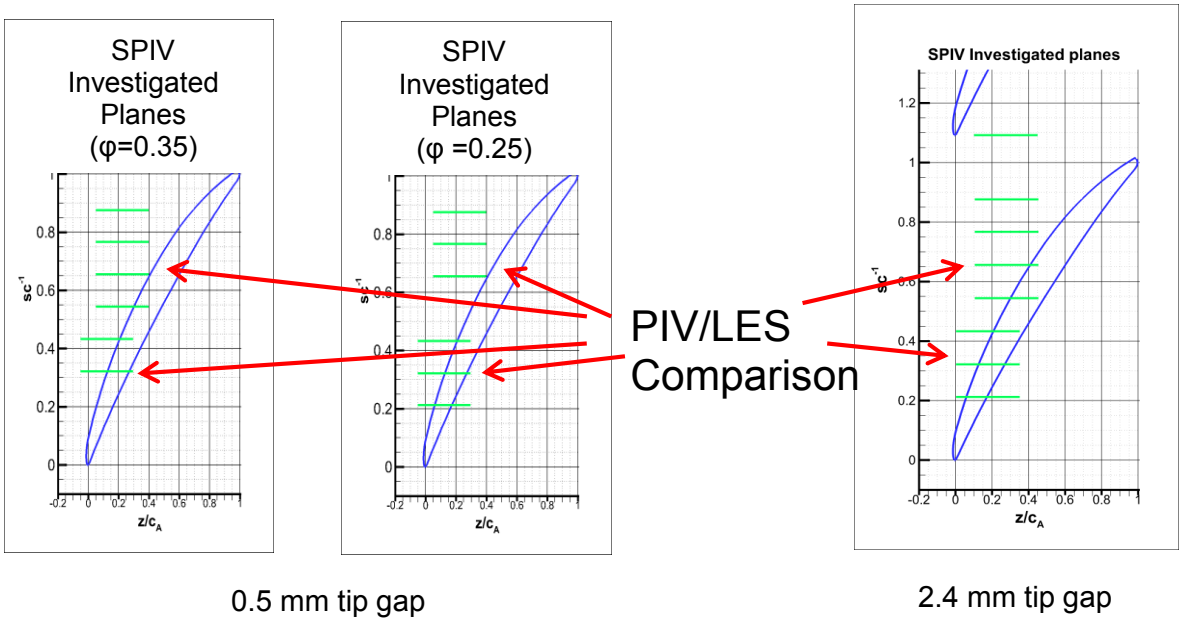

FIGURE 13. PIV MEASUREMENT, MERIDIONAL PLANES

COMPARISON OF TIP CLEARANCE FLOW STRUCTURES BETWEEN PIV AND LES

Measured instantaneous velocity vectors and corresponding vorticity contours are compared with the LES results at the meridional plane, which is 32.8 % downstream from the leading edge for the three flow conditions in Figures 10, 11, and 12. The measured data is from the Stereoscopic PIV (SPIV) technique. Details of the SPIV measurement are given by Li et al. [2015]. SPIV measurement planes are shown in Figure 13. Instantaneous flow structures from the LES matches fairly well with the PIV data. The results in Figures 10-12 show many interesting features of the tip clearance vortex. The instantaneous velocity vectors and the vorticity contours in Figures 10, 11 and 12 illustrate the detailed mechanism of tip vortex generation. First of all, tip clearance vortex is not a clearly defined single vortex structure. Rather the tip clearance vortex is a system of interlaced vorticities. When averaged over time, the tip vortex structure becomes similar to the traditional single vortex structure. Figure 14 illustrates how the tip clearance vortex is generated. The counter-clockwise rotating vortex is formed from the shear layer on the immediate top of the blade. Fluid near the top of the blade in this shear layer is convected by the tip flow and turned radially inward as it meets the incoming main flow. On the other hand, fluid near the casing forms a clockwise rotating vortex (blue colored vortex core) as it meets the incoming main flow and moves outside of the main vortex, as shown in the LES simulation.

When the flow rate is decreased to near stall with the small tip gap (0.5 mm), the tip clearance core vortex starts earlier near the leading edge and moves further away from the suction side. This is due to larger pressure difference across the blade near the leading edge. Also, the tip clearance core vortex moves further inward in the radial direction. On the other hand, the tip clearance core vortex stays closer to the suction side when the tip gap is increased at the peak efficiency condition.

Figures 15, 16, and 17 compare instantaneous velocity vectors and vorticity distributions at the meridional plane, 65.5 % downstream. The vorticity contours show that the tip clearance core vortex moves further away from the blade suction side and further radially inward when the flow rate is decreased with the small tip gap (0.5mm). When the tip gap is increased from 0.5 mm to 2.4 mm, the tip clearance core vortex remains closer to the blade. With the larger tip gap, more tip gap flow adds to the circulation and the tip core vortex stays stronger compared to that of the 0.5 mm tip gap.

Instantaneous velocity vectors inside the tip gap at the same meridional plane for three flow conditions are compared in Figure 18. With a 0.5 mm tip gap, instantaneous velocity distributions show that the flow is primarily driven by the pressure differences across the blade tip section. The velocity vectors are almost uniform, except very close to the blade tip. As illustrated in Figure 18, flow separation and reattachment are calculated near the entrance of the tip gap as many previous studies have indicated. This recirculating area is much smaller and confined close to rotor tip. The SPIV was not set up to measure the boundary layer for the current test and the calculated recirculating area is located between the rotor tip and the first SPIV plane.

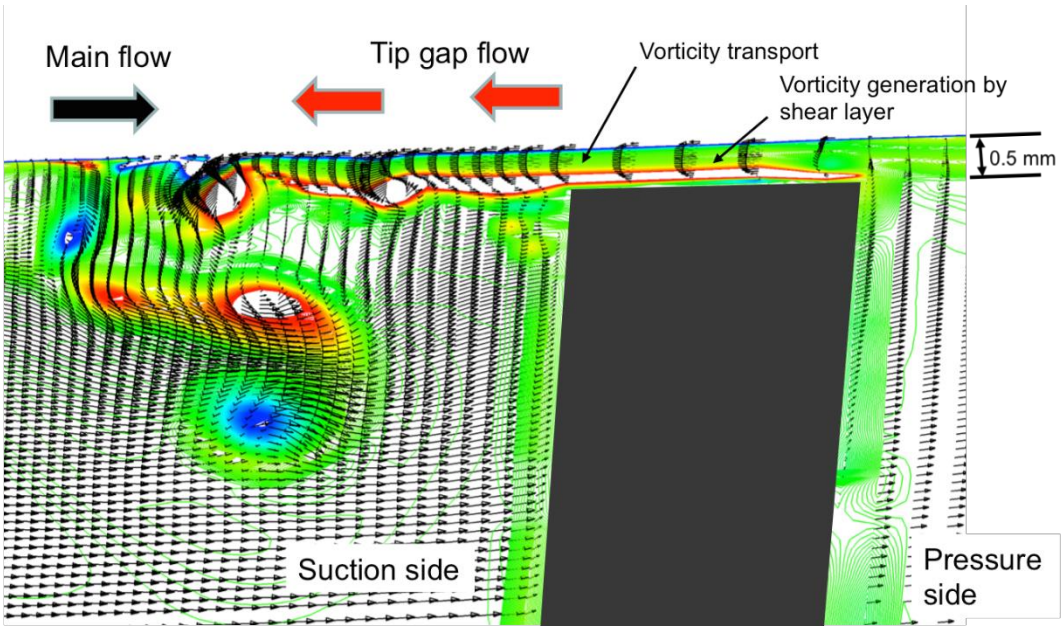

FIGURE 14. GENERATION OF TIP CLEARANCE VORTEX

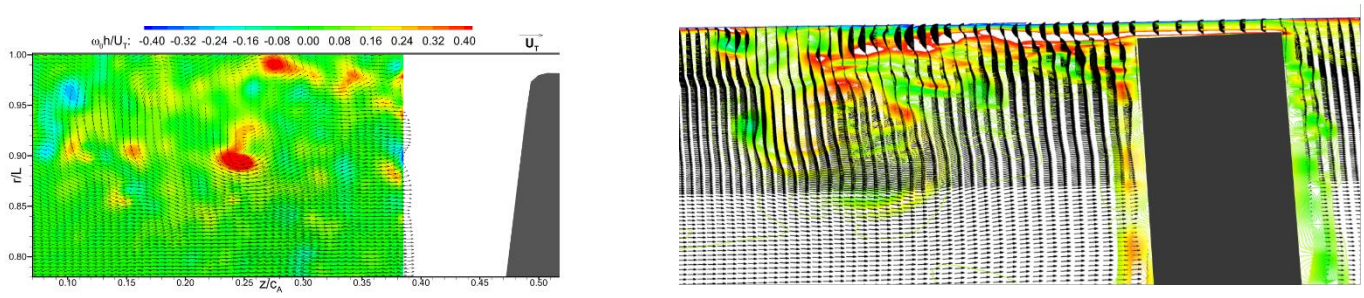

FIGURE 15. COMPARISON OF INSTANTANEOUS VELOCITY VECTORS AND VORTICITY, s/C = 0.655, 0.5 mm GAP, AT DESIGN CONDITION

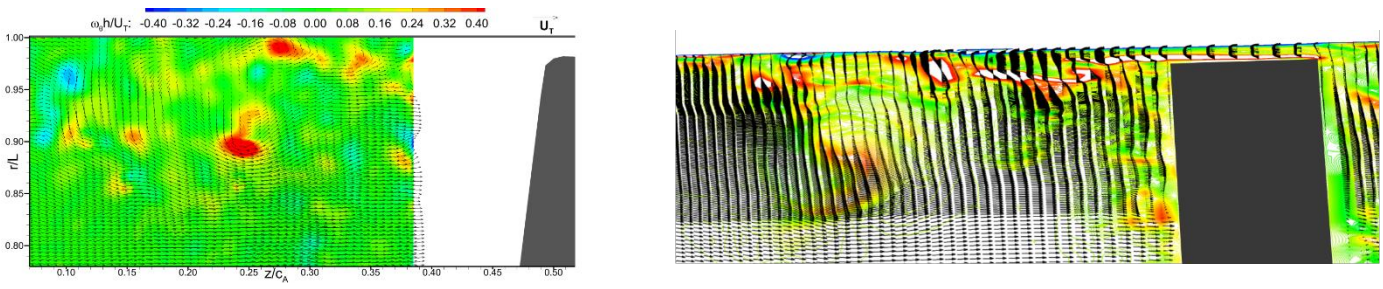

FIGURE 16. COMPARISON OF INSTANTANEOUS VELOCITY VECTORS AND VORTICITY, s/C = 0.655, 0.5 mm GAP, AT NEAR STALL

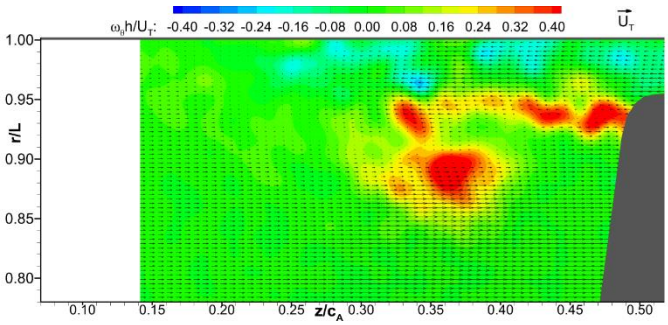

SPIV

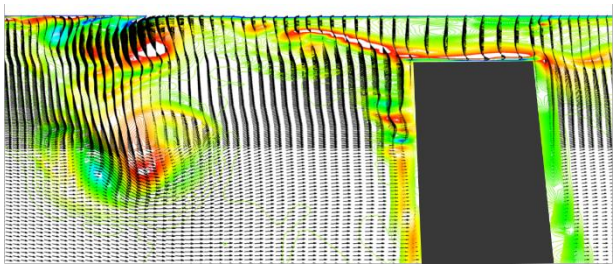

LES

FIGURE 17. COMPARISON OF INSTANTANEOUS VELOCITY VECTORS AND VORTICITY, s/C = 0.655, 2.4 mm GAP, AT DESIGN CONDITION

FIGURE 18a. INSTANTANEOUS VELOCITY VECTORS INSIDE TIP GAP, 0.5 mm GAP, s/C = 0.328, AT DESIGN CONDITION

FIGURE 18b. INSTANTANEOUS VELOCITY VECTORS INSIDE TIP GAP, 0.5 mm GAP, s/C = 0.328, AT NEAR STALL CONDITION

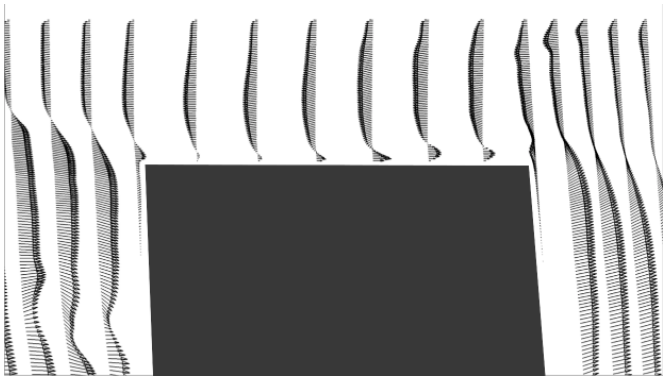

FIGURE 18c. INSTANTANEOUS VELOCITY VECTORS INSIDE TIP GAP, 2.4 mm GAP, s/C = 0.328, AT DESIGN CONDITION

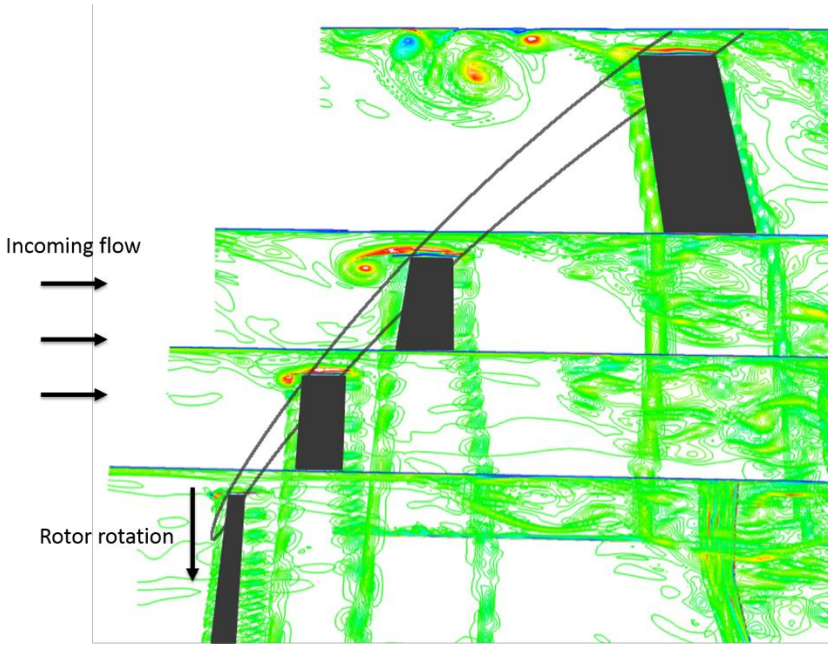

FIGURE 19. INSTANTANEOUS VORTICITY DISTRIBUTION AT FOUR MERIDIONAL PLANES

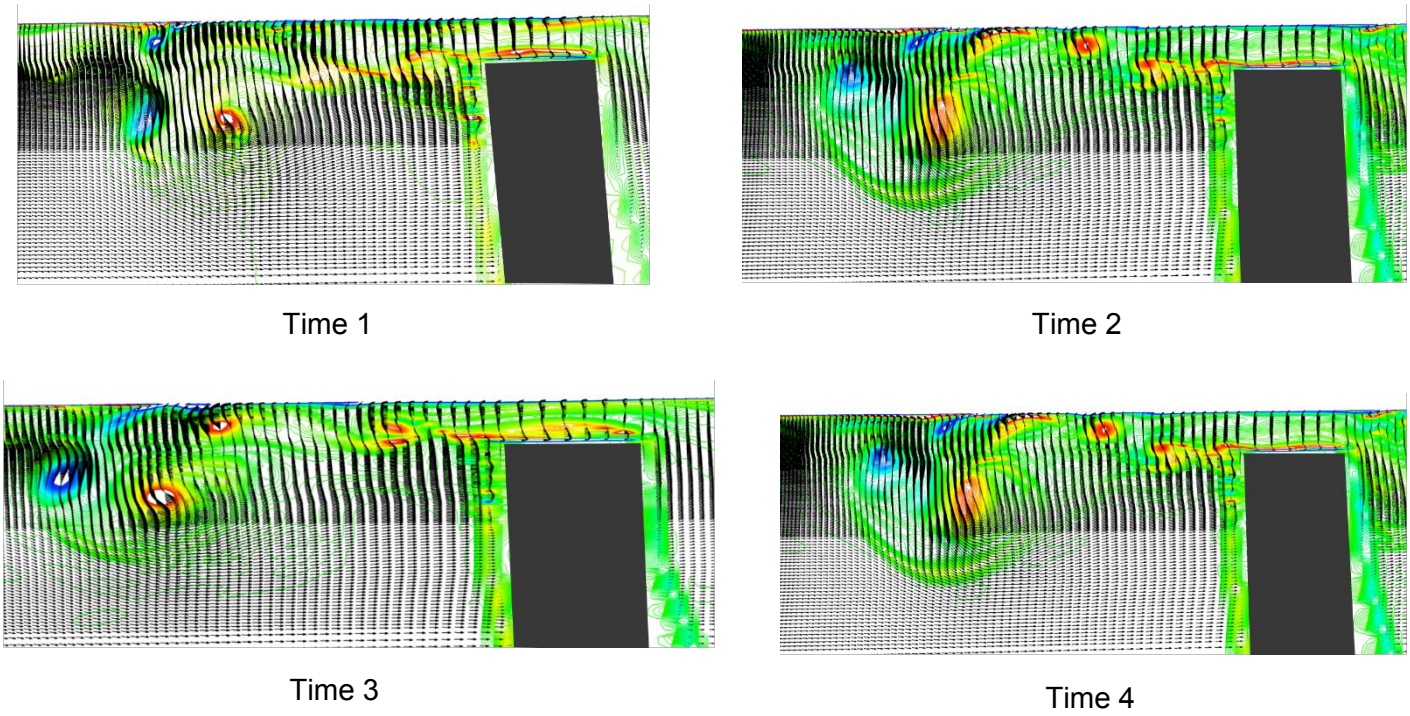

FIGURE 20. CHANGES IN VORTICITY DISTRIBUTION, 2.4 mm, s/C = 0.655, AT DESIGN FLOW CONDITION

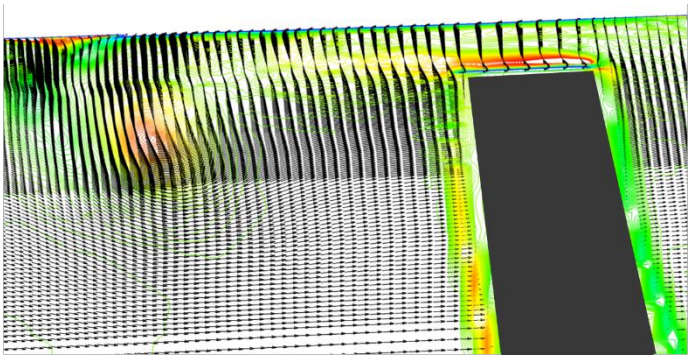

FIGURE 21. TIME-AVERAGED VORTICITY DISTRIBUTION, 2.4 mm, s/C = 0.655 AT DESIGN FLOW CONDITION

The velocity distribution becomes much more complex when the tip gap is increased, as shown in Figure 18. For the smaller tip gap, LES velocity vectors inside tip gap agree very well with the PIV measurement. For the larger tip gap, the LES velocity profile agrees fairly well with the PIV above 20% of the tip gap. Near the blade top, LES calculates a reversed flow region which PIV does not support. As shown in Figure 10, the LES used a sharp tip corner geometry. On the other hand, the actual tip corner geometry for the SPIV is round due to the manufacturing process. This difference in rotor tip geometry might contribute to the discrepancy. Instantaneous vorticity distributions at several meridional planes are shown in Figure 19. This figure shows how the tip core vortex is generated and convected downstream. As shown in Figure 19, more vorticities are added by the shear layer on the rotor tip downstream of the leading edge.

Figure 20 compares changes in the vorticity distribution at the 65.5 % meridional plane between PIV and LES. Both PIV and LES show a similar trend. With time, both the location and the strength of the core vortex changes significantly. The time averaged vorticity distribution from the LES is given in Figure 21. The time-averaged tip clearance vortex in Figure 21 is a typical tip clearance vortex structure from steady simulation. However, the real instantaneous tip clearance flow structures are quite different from the time-averaged flow field. Actually, the time-averaged tip clearance flow structure shown in Figure 21 never occurs in reality.

CONCLUDING REMARKS

The unsteady tip clearance flows in a low speed one and a half stage axial compressor with two different tip gaps are investigated with PIV measurement and a Large Eddy Simulation. Detailed changes in the tip clearance flow structures when the tip gap is increased from 0.5 mm (0.49 % of tip chord) to 2.4 mm (2.34% of tip chord) at the design operating condition are investigated along with the changes when the flow rate is reduced to near stall with the 0.5 mm tip gap. Both the PIV measurement and the LES show that tip clearance vortex is not a single vortex structure as commonly understood. The tip clearance vortex is a structure with multiple interlaced vorticities and it never rolls up to a single structure. The strong shear layer at the immediate top of the rotor blade is convected with the tip clearance flow and is bent radially inward when the tip clearance flow collides with the incoming main flow, which forms the tip clearance core vortex. The tip clearance flow is inherently unsteady due to the interaction among the interlaced vortices. When averaged over time, the averaged tip clearance flow looks like a traditional tip clearance flow with a single fixed vortex structure. However, this averaged tip vortex structure does not occur in reality. Strategies to control the generation of aerodynamic loss and noise generation should be based on the instantaneous tip flow structure rather than an averaged flow structure. When the tip gap is increased at the design flow condition, the tip clearance vortex structure remains closer to the blade with the stronger tail of the vortex structure. When the flow rate is reduced to near stall condition, the tip clearance vortex structure occurs further upstream and moves away from the blade suction side and it travels radially further inward.

REFERENCES

Bergner, J., Matthias, K, Schiffer, H.P., and Hah, C., 2006, "Short Length-Scale Rotating Stall Inception in a Transonic Axial Compressor – Experimental Investigation," ASME Paper GT2006-90209.

Chen, J.P., Hathaway, M.D., and Herrick, G.P., 2008, "Prestall Behavior of a Transonic Axial Compressor Stage via Time-Accurate Numerical Simulation," ASME Journal of Turbomachinery, Vol. 30, October 2008.

Germano, M., Piomelli, U., Moin, P., and Cabot, W. H., 1991, "A Dynamic Subgrid-Scale Eddy-Viscosity Model," Journal of Fluid Mechanics, Vol. A3, pp. 170-176.

Hah, C., 1986, "A Numerical Modeling of Endwall and Tip-Clearance- Flow of an Isolated Compressor ," ASME Journal of Engineering for Gas Turbines and Power Vol. 108, No. 1, pp. 15-21.

Hah, C. and Shin, H., 2012, "Study of Near –Stall Flow Behavior in a Modern Transonic Fan with Compound Sweep," ASME Journal of Fluids Engineering, Vol. 134, pp.071101-071107.

Hoying,D.A., Tan, C.S., Vo, H.D., and Greitzer, E.M., 1999, "Role of blade passage flow structure in axial compressor rotating flow inception," ASME J. of Turbomachinery, 121,pp.735-742.

Inoue, M., Kuromaru, M, Yoshida, S., Minami, T., Yamada, K., and Furukawa, M., 2004, "Effects of Tip Clearance on Stall Evolution Process in a Low-Speed Axial Compressor Stage," ASME Paper GT2004-5335.

Kielb, R. E., Barter, J. W., Thomas, J., and Hall, K. C., 2003, "Blade Excitation by Aerodynamic Instabilities–A Compressor Blade Study," ASME Paper GT2003-38634.

Maerz, J., Hah, C., and Neise, W, 2002, "An Experimental and Numerical Investigation into the Mechanism of Rotating Instability," ASME Journal of Turbomachinery, Vol. 124, pp. 367-375.

Mailach, R., Lehmann, I., and Vogeler, K., 2000, "Rotating Instabilities in an Axial Compressor Originating from the Fluctuating Blade Tip Vortex," ASME Paper 2000-GT.

Pullan, G., Young, A.M., Day, I.J., Greitzer, E.M., Spakovszky, Z.S., 2013, “Origins and Structure of Spike-Type Rotating Stall,” ASME paper 2012-68707.

Smith L. H. Jr., 1993, Private communication.

Tan, D., Yuanchao, L., Wilkes, I., Miorini, R.L., and Katz, J., 2014, “Visualization and Time Resolved PIV Measurements of the Flow in the Tip region of a Subsonic Compressor Rotor,” ASME Paper GT2014-27195.

Tan, D., Yuanchao, L., Chen, H., Wilkes,I., and Katz, J., 2015, “The Three Dimensional Flow Structure and Turbulence in the Tip Region of an Axial Compressor,” ASME Paper GT2015-43385.

Vo, H. D., Tan, C. S., and Greitzer, E. M., 2005, “Criteria for Spike Initiated Rotating Stall,” ASME Paper GT2005-68374.

Li, Y., Tan, D., Chen, H., and Katz, J., 2015, “Effects of Tip Gap Size on the Flow Structure in the Tip Region of an Axial Turbomachine,” ASME paper, AJK2015-140787.

Yamada, K, Kikuda, H.,Furukawa, Kunjishima, S., and Hara, Y., 2013, “Effects of Tip Clearance on the Stall Inception Process in an Axial Compressor Rotor,” ASME Paper GT-2013-95479.

Wasserbauer, C. A., Weaver, H. F., and Senyitko, R. G., “NASA Low-Speed Axial Compressor for Fundamental Research, “NASA TM 4635, Feb. 1995.

Weichert, S. and Day, I, 2013, “Detailed Measurements of Spike Formation in an Axial Compressor,” ASME paper GT2013.

Wellborn, S. R., Okiishi, T. H., “Effects of Shrouded Stator Cavity Flows on Multistage Axial Compressor Aerodynamic Performance,” NASA Contractor Report 198536, October 1996.

Wisler, D. C., “Core Compressor Exit Stage Study: Volume 1-Blade Design,” NASA CR

Wu, H., Tan, D., Miorini, R.L., and Katz, J., 2011, “Three-Dimensional Flow Structures and Associated Turbulence in the Tip Region of a Water Jet Pump Rotor,” Exp. Fluids, 51(6), pp. 1721-1737.